Research Article | Vol. 28, No. 17 / 17 August 2020 / Optics Express 24919
Optics EXPRESS

High optical nonlinearity in low-dimensional halide perovskite polycrystalline films

WEI-YUN LIANG,[1] FANGZHOU LIU,[2] YU-JUNG LU,[3] JASMINKA POPOVIĆ,[4] ALEKSANDRA DJURIŠIĆ,[2] AND HYEYOUNG AHN[1,*]

[1]*Department of Photonics, College of Electrical and Computer Engineering, National Chiao Tung University, Hsinchu 30010, Taiwan*
[2]*Department of Physics, University of Hong Kong, Pokfulam Road, Hong Kong, China*
[3]*Research Center for Applied Sciences, Academia Sinica, Taipei 11529, Taiwan*
[4]*Center of Excellence for Advanced Materials and Sensing Devices, Division for Materials Physics, Laboratory for Synthesis and Crystallography of Functional Materials, Ruđer Bošković Institute, Bijenička 54, Zagreb, Croatia*
[*]*hyahn@mail.nctu.edu.tw*

Abstract: The nonlinear optical properties of low-dimensional polycrystalline halide perovskite films consisting of ethylammonium (EA) and butylammonium (BA) cations are investigated using Z-scan technique. Across the band-edge, two-dimensional $(BA)_2PbI_4$ exhibits a transition from saturable absorption (SA) to reverse-SA and its nonlinear absorption and nonlinear refractive index are much smaller than those of bulk counterparts. Meanwhile, $EAPbI_3$ with one-dimensionality of the inorganic structure shows the SA behavior both above and below band-edge and the estimated nonlinear optical parameters of polycrystalline $EAPbI_3$ are comparable to those of single-crystalline ones, attributed to high dielectric contrast between the inorganic and organic elements in one-dimensional structures.

1. Introduction

Depending on the choice of organic and inorganic elements, metal halide perovskites can have tunable bandgaps and different structural forms. Recently, low-dimensional (0D, 1D or 2D) halide perovskites realized by introducing long chained cations as barriers between inorganic octahedra frameworks have attracted much attention owing to their excellent optical properties for photovoltaic and optoelectronic applications [1–5]. In particular, strong quantum confinement effect in low-dimensional halide perovskites enables the tunable and narrow excitonic emission at room temperature. Furthermore, exciton effect in low-dimensional perovskites leads to higher nonlinear optical responses than those in three-dimensional phase [6–9]. High formation energy, as well as the hydrophobic property of organic cations, also improve the stability of low-dimensional perovskites in an ambient atmosphere, extending their commercial utility into new areas such as large area, stable nonlinear optical devices [10].

All-optical switches based on nonlinear optics operate at high speeds and provide broad bandwidth unattainable by conventional electronic switches. Nonlinear materials used for optical switches are required to have not only large optical nonlinearity, but also fast carrier recovery time. In this work, we have investigated the nonlinear optical properties of low-dimensional perovskites consisting of the two alkylammonium cations, n-butylammonium (BA) and mono-ethylammonium (EA), near the bandgap using the conventional Z-scan method. Utilization of BA and EA cations results in the formation of 2D layered and 1D chain-like perovskites with bandgaps near 2.35 eV [11], allowing the development of nonlinear optical devices operating in visible spectral range. However, the reported values of nonlinear optical parameters (both nonlinear absorption coefficient and nonlinear refractive index) of low-dimensional perovskites are widely scattered due to the variation in crystalline quality of perovskites and moreover, their crystal

#394172 https://doi.org/10.1364/OE.394172
Journal © 2020 Received 31 Mar 2020; revised 6 Jun 2020; accepted 28 Jul 2020; published 10 Aug 2020

Optics EXPRESS

structure-dependence have not yet been reported [6–9]. To date, the highest optical nonlinearities for low-dimensional perovskites have been reported for single-crystalline perovskite nanosheets [9], but engineering of these nanosheets using mechanical exfoliation method from bulks hampers the development of large-scale nonlinear optical devices. Our results on $(BA)_2PbI_4$ thin films show that the optical nonlinearity is still influenced by the crystalline quality of films and the estimated nonlinear optical parameters are smaller than those of single-crystalline counterparts [9]. Meanwhile, despite its polycrystalline nature, 1D $EAPbI_3$ thin films exhibit much larger optical nonlinearity at lower input intensities than $(BA)_2PbI_4$ films and its value is comparable to that of single-crystalline perovskite nanosheets. Ultrafast pump-probe experiment shows that both $EAPbI_3$ and $(BA)_2PbI_4$ exhibit optical bleaching and the recovery times are less than a few picoseconds, which makes them an excellent candidate to realize the ultrafast all-optical switching.

2. Experimental methods

The $EAPbI_3$ and $(BA)_2PbI_4$ perovskite films were synthesized by spin-coating method as previously described [11]. Briefly, precursor solutions were prepared by dissolving the precursor chemicals in a solvent mixture of *N,N*-Dimethylformamide (DMF, anhydrous, 99.9+%, Alfa Aesar) and dimethyl sulfoxide (DMSO, anhydrous, 99.8+ %, Alfa Aesar) at a concentration of 0.5M. For the preparation of $EAPbI_3$, ethyl ammonium iodide (EAI, Greatcell Solar Ltd.) and PbI_2 (99.9985%, Alfa Aesar) were dissolved in a molar ratio of 1:1 in the mixture of DMF and DMSO (5:1 volume ratio). For $(BA)_2PbI_4$, *n*-butylammonium iodide (BAI, Greatcell Solar Ltd.) and PbI_2 are dissolved in a molar ratio of 2:1 in the solvent mixture of DMF and DMSO (3:1 volume ratio). Before spin-coating, the substrates were sonicated for 10 min in acetone, toluene, acetone, ethanol, and deionized water, respectively, and treated with oxygen plasma immediately before use. The films were then prepared by spin-coating the precursor solution on clean substrates at 5000 rpm for 30 s inside an argon-filled glovebox, followed by drying in low vacuum for 1 min. and annealing at 120 °C for 10 min to remove the solvent. In order to prevent degradation of samples in an ambient environment, all perovskite samples used in our study were encapsulated by a thin quartz glass. The morphology of perovskites was studied by scanning electron microscopy (SEM, JSM-7000F) and their crystal structures were investigated by using an X-ray diffractometer (XRD, Bede D1) with monochromatic Cu-Kα radiation (λ=1.5406 Å). Le-Bail fitting was used for indexing and determination of the lattice parameters. The third-order nonlinear absorption coefficient (β) and nonlinear refraction coefficient (n_2) were obtained via open-aperture (OA) and closed-aperture (CA) Z-scan configurations [12]. Two photodetectors are used for simultaneous measurement of OA and CA signals during the scanning process. A femtosecond Ti:sapphire laser (1 kHz repetition rate and 100 fs pulse duration) was used as the excitation and probe light source for Z-scan measurement and ultrafast pump-probe experiment. The nominal thickness of our perovskite films is ~300 nm that is much smaller than the Rayleigh length (z_0) of ~2 mm. The Z-scan as well as carrier dynamics measurements were repeatedly measured for several sets of samples synthesized under the same growth conditions. The quality of samples were confirmed by XRD and low-temperature photoluminescence measurements [11].

3. Results and discussion

Figure 1(a) and (b) illustrate the top-view scanning electron micrograph (SEM) images of $EAPbI_3$ and $(BA)_2PbI_4$ films. $EAPbI_3$ film shows elongated granular morphology, whereas $(BA)_2PbI_4$ shows close-packed uniform surface with a fine texture. The sheet-like morphology in $(BA)_2PbI_4$ characterizes the growth of two-dimensional layered films. Figure 1(c) shows the X-ray diffraction (XRD) curves of $EAPbI_3$ and $(BA)_2PbI_4$ films on quartz substrate. XRD structural analysis revealed that $EAPbI_3$ crystallizes within the orthorhombic lattice with $a = 8.618(4)$ Å, $b = 8.030(7)$ Å, and $c = 30.119(5)$ Å, similar to the structure reported by Park *et al.* [13]. The

Optics EXPRESS

structure of $(BA)_2PbI_4$ has been refined in orthorhombic space group and exhibits the periodicity b=27.631(1) Å along the b-direction, which is typical for 2D perovskites showing a preferential growth along one direction [2].

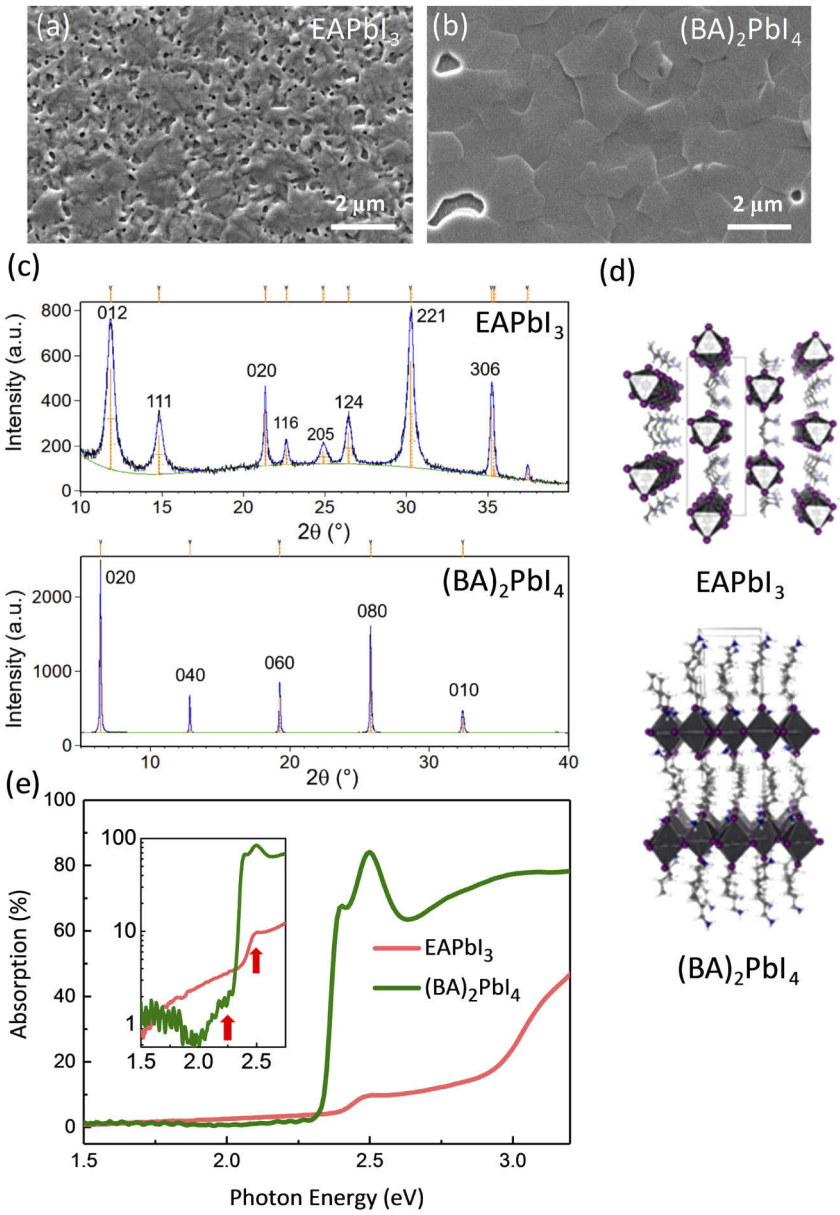

Fig. 1. (a),(b) Top-view SEM images, (c) XRD curves, and (d) Schematic views of crystal structures of the $EAPbI_3$ and $(BA)_2PbI_4$ perovskite films. Symbols in (d) represent Pb and its polyhedra in grey, iodide in purple, and nitrogen in blue. (e) Absorption spectra $EAPbI_3$ and $(BA)_2PbI_4$. Inset in (e) shows the same absorption spectra in logarithmic scale and red arrows indicate the wavelengths chosen for Z-scan measurement.

Figure 1(d) illustrates the schematics of crystal structures of $EAPbI_3$ and $(BA)_2PbI_4$ which depict 1D and 2D arrangements of inorganic octahedron cages separated by alkyl chains of

Optics EXPRESS

different lengths. In $EAPbI_3$, inorganic octahedra construct 1D networks via face-sharing connectivity, while in $(BA)_2PbI_4$, corner-sharing inorganic cages form 2D layered structure. Different dimensionality is likely to lead to different physical properties, which are strongly depending on the nature of the cationic elements. Figure 1(e) shows the optical absorption spectra of $EAPbI_3$ and $(BA)_2PbI_4$ measured at room temperature. Their direct bandgap properties are characterized by the clear absorption edges locating near 2.35 eV along with the narrow excitonic absorption peaks, particularly pronounced in $(BA)_2PbI_4$, reflecting the exciton confinement effect in low-dimensional structures. Meanwhile, as can be seen in the inset of Fig. 1(e), the absorption edge of direct-bandgap semiconductor $(BA)_2PbI_4$ is very steep, whereas the excitonic absorption in $EAPbI_3$ is relatively weak and there is a reasonable amount of absorption below the band edge.

In order to investigate the optical nonlinear properties, the Z-scan measurements were carried out at wavelengths 500 and 550 nm (two arrows in the inset of Fig. 1(a)). These excitation wavelengths were chosen to probe the nonlinear properties above and below the absorption edge for both samples. Figure 2 shows the typical OA and CA Z-scan data of $(BA)_2PbI_4$ excited at 500 and 550 nm. In Fig. 2(a), upon excitation at 500 nm where the one-photon absorption dominates, the saturable absorption (SA) behavior is observed and the maximum transmittance at z=0 increases nonlinearly as the excitation power density increases. For the below-bandgap excitation at 550 nm, the Z-scan traces in Fig. 2(b) shift to the reverse-saturable absorption (RSA). CA Z-scan data in Fig. 2(c) and (d) also exhibit a transition from self-focusing to self-defocusing behavior under excitation above and below the exciton resonance. The Z-scan data from the bare quartz substrate (black symbols) in Fig. 2(b) confirms that there is no noticeable contribution from the substrate under the same excitation conditions. (CA Z-scan data of substrate are similar and not shown here.) In Z-scan data, scattered data and systematic asymmetry in baselines is often caused by laser instability and surface imperfection and can be corrected by the low intensity background responses [14,15]. Some features appearing in the wing in Fig. 2(b) are possibly due to higher-order nonlinearity.

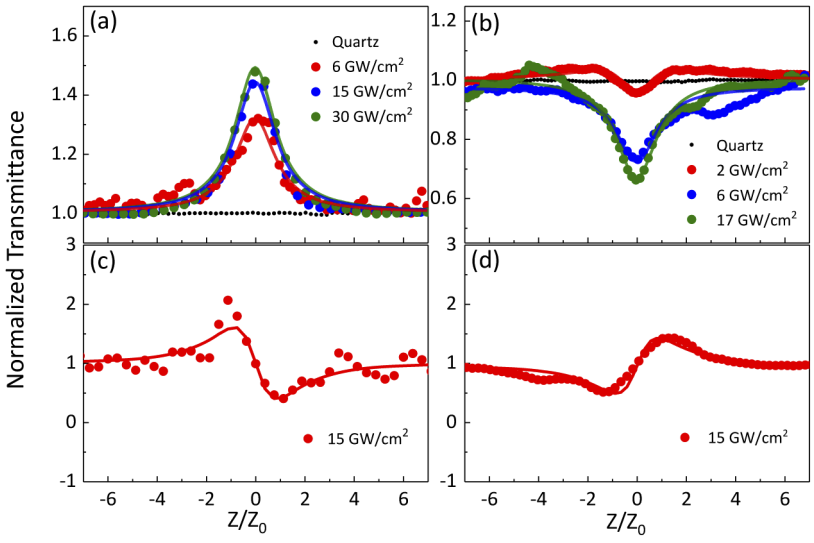

Fig. 2. OA [(a) and (b)] and CA [(c) and (d)] Z-scan traces of $(BA)_2PbI_4$. (a) and (c) are measured at 500 nm and (b) and (d) are at 550 nm, respectively. Solid curves are the best-fitting results calculated by using formulae in the text.

Optics EXPRESS

The transmitted light intensity (I) through the material can be described by [16–18]

$$\frac{dI}{dz} = -[\alpha_0 + \beta(I)I]I, \tag{1}$$

where z is the propagating distance in the sample, α_0 is the linear absorption coefficient, $\beta(I)$ is the intensity-dependent nonlinear absorption coefficient, typically defined as $\beta(I) = \beta_0/\left(1 + \frac{I}{I_s}\right)$, with I_s the saturable intensity and β_0 the nonlinear absorption coefficient under the low-intensity limit [16]. For saturable absorption, β is a negative value, while for reverse-saturable absorption, such as excited state absorption or two-photon absorption, β is positive. Combining with Gaussian intensity profile of laser beam, one can obtain the expression to fit the z-dependent normalized OA Z-scan data [19],

$$T_{OA}(z) = 1 - \frac{q_0}{2\sqrt{2}(1 + z^2)}, \tag{2}$$

where $q_0 = \beta I_0 L_{eff}$, L_{eff} is the effective length of the sample calculated by $L_{eff} = \frac{1-e^{-\alpha_0 L}}{\alpha_0}$ and L is the active length (~300 nm) of the sample. In the fitting process, β is a fitting parameter, while α_0 obtained from the optical transmission spectra is fixed to be 3.3×10^3 and 5.7×10^4 cm^{-1} for $EAPbI_3$ and $(BA)_2PbI_4$, respectively. From the best-fits to experimental data (solid curves in Fig. 2(a) and (b)), β at $I = 6$ GW/cm^2 are estimated to be −5.3 cm/MW and 4.3 cm/MW for SA and RSA responses, respectively. These values are about two orders of magnitude larger than those of $(BA)_2PbI_4$ in powder form [7], but are similar to those of another kind of 2D perovskite, phenylethylamine lead iodide ($(PEA)_2PbI_4$) thin film [8].

The CA (normalized to OA) Z-scan curves in Fig. 2(c) and (d) are fitted by using the relation given as [20,21]

$$T_{CA}(z) = 1 + \frac{4\Delta\Phi z}{(1 + z^2)(9 + z^2)}, \tag{3}$$

where $\Delta\Phi = kI_0 L_{eff} n_2$ is the phase shift, $k = 2\pi/\lambda$ is the wavevector at the pump wavelength λ, and the intensity dependence of refractive index is defined via $n(I) = n_0 + n_2 I$. The estimated value of n_2 at I ~15 GW/cm^2 for $(BA)_2PbI_4$ films is shifted from -5.2×10^{-11} to 3.5×10^{-11} cm^2/W at wavelengths above (500 nm) and below (550 nm) the absorption edge.

Figure 3 depicts the Z-scan data of 1D $EAPbI_3$ films measured at 500 and 550 nm. Unlike the results of $(BA)_2PbI_4$, both OA Z-scan curves in Fig. 3(a) and (b) show SA responses without sign-flip of β. The CA Z-scan profiles in Fig. 3(c) and (d) also do not show the transitional behavior, instead, exhibit only self-focusing behavior. Using Eq. (2), β at the excitation wavelength λ_e =500 nm is estimated to be −240 cm/MW for I=1.5 GW/cm^2, while at 550 nm, it becomes −10 cm/MW. The values of β for $EAPbI_3$ and $(BA)_2PbI_4$ are much larger than those of other 2D materials, such as graphene (−0.09 cm/MW) [22] and the saturable intensities are several orders of magnitude larger than that of gallium arsenide (~79 GW/cm^2) [23].

Besides excitation wavelength, nonlinear optical parameters are functions of the excitation laser intensity and we summarized their relation in Fig. 4(a)–(c). Solid curves in Fig. 4(a) and (b) are obtained from the relation above with fitting parameters listed in Table 1. Fitting parameters of $(BA)_2PbI_4$ used in Fig. 4(a) are β_0 = −9.6 and 10.1 cm/MW and I_s ~6.4 and 4.2 GW/cm^2 for SA and RSA responses, respectively. As is mentioned above, these values are similar to that of 2D $(PEA)_2PbI_4$ films [8]. It was also reported that $(PEA)_2PbI_4$ flakes mechanically exfoliated from bulk materials have much higher nonlinear coefficients than polycrystalline thin films [8], indicating that the nonlinear optical parameters of perovskites are strongly influenced by the crystalline quality of samples. Meanwhile, another Z-scan measurement of single-crystalline $(BA)_2PbI_4$ nanosheets which were also prepared by mechanical exfoliation method shows the transition in sign for both β_0 and n_2 near the plasma frequency (ω_p) and in particular, β becomes significantly large (< −250 cm/MW) for low intensity excitation [9].

Optics EXPRESS

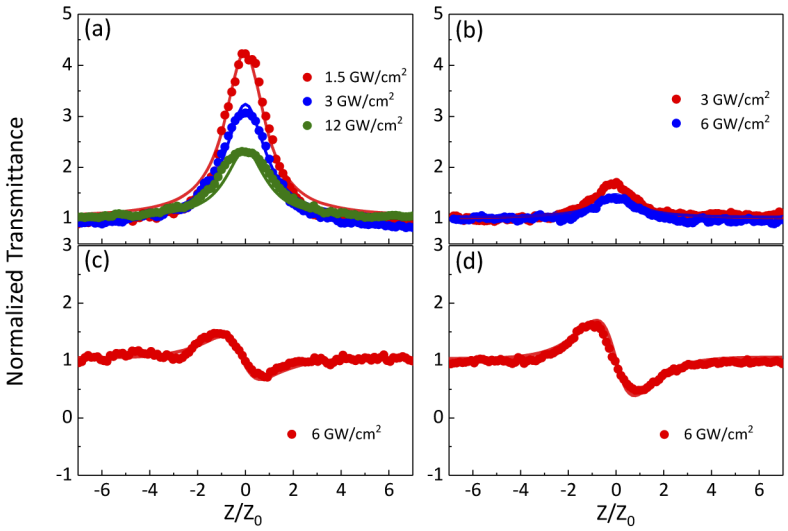

Fig. 3. OA [(a) and (b)] and CA [(c) and (d)] Z-scan traces of $EAPbI_3$. (a) and (c) are measured at 500 nm and (b) and (d) are at 550 nm, respectively. Solid curves are the best-fitting results calculated by using formulae in the text.

Table 1. Nonlinear optical parameters used in the text

Material	Pump Wavelength (nm)	Nonlinear absorption	β_0 (β_0') (cm/MW)	I_s ($I^2_{s,\beta'}$) (GW/cm^2)	n_2 (cm^2/W)
$(BA)_2PbI_4$	500	SA	-9.6 ± 0.7	6.4 ± 0.8	-5.2×10^{-11}
	550	RSA	10.1 ± 1.4	4.2 ± 0.7	7.1×10^{-11}
$EAPbI_3$	500	SA	-310 ± 70 (-216)	1.5 ± 0.4 (0.65)	-3.2×10^{-10}
	550	SA	-18.5 ± 3.5	6.8 ± 1.0	-2.3×10^{-10}

Interestingly, from the curve fitting in Fig. 4(b), β_0 of $EAPbI_3$ excited at 500 nm is estimated to be as large as -310 cm/MW with much smaller saturation intensity of 1.5 GW/cm^2. It is noteworthy that this large β_0 is obtained from polycrystalline $EAPbI_3$ films fabricated by spin-coating method. The nonlinear absorption coefficient significantly decreases as the excitation light intensity increases above the saturatble intensity. We also notice that the solid curve in Fig. 4(b) obtained by applying the simple saturable absorption model cannot properly fit the sharp increase (negative value) of β at low intensity. Similarly drastic increase of β at low intensity and the disagreement with the saturable absorption model were previously observed for single crystalline $(BA)_2PbI_4$ and $(PEA)_2PbI_4$ [8,9], implying that it is requisite to employ a higher-order nonlinear relation to describe the intensity dependence of nonlinear absorption in high quality low-dimensional perovskites. A plausible fitting to experimental results (dashed line) could be obtained by employing an extended SA model with the additional relation of $\beta_0'/\left(1+\frac{I^2}{I^2_{s,\beta'}}\right)$, which has been used to describe the homogeneously broadened system [8,16]. However, it is still an empirical postulation and detailed explanation needs further experimental and theoretical investigation.

A large enhancement of nonlinear absorption in low-dimensional materials is well accepted to be attributed to the resonant enhancement of locally confined excitons [9,16,24]. Excitons in $(BA)_2PbI_4$ films are tightly localized within 2D layered structures and this strong quantum confinement of excitons leads to a large exciton binding energy (>600 meV) and enables intense

Optics EXPRESS

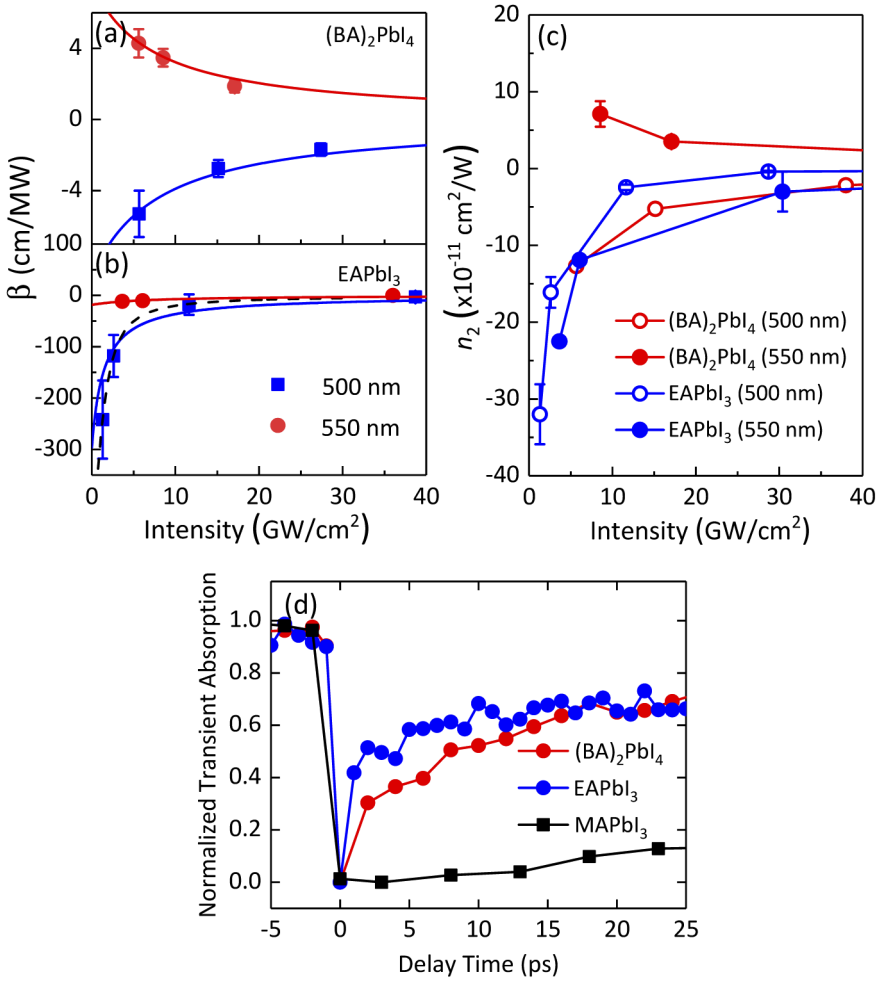

Fig. 4. Excitation light intensity dependence of nonlinear optical coefficients. (a) and (b) are β for $(BA)_2PbI_4$ and $EAPbI_3$ perovskites, respectively, and (c) is n_2 for both samples. (d) Normalized transient absorption of $(BA)_2PbI_4$ and $EAPbI_3$, compared with that of 3D $MAPbI_3$.

excitonic emission [11]. However, our results show that $EAPbI_3$ with much smaller exciton binding energy (~33 meV) possesses higher optical nonlinearity than $(BA)_2PbI_4$, and it is necessary to consider another approach including dielectric properties [25]. As is depicted in Fig. 1(d), the spin-coated $EAPbI_3$ film forms a one-dimensional chain structure containing face-sharing PbI_6 octahedra. Since these chain structures are surrounded by organic cation barriers, the dielectric contrast between the inorganic and organic elements in 1D $EAPbI_3$ can be high and may not be strongly influenced by the crystalline quality of films compared to the layered $(BA)_2PbI_4$ films, for which the exciton confinement is limited to the direction of layer stacking axis. Therefore, combined with the quantum confinement effect, strong dielectric confinement in $EAPbI_3$ films may lead to higher optical nonlinearity under much lower intensity excitation than in $(BA)_2PbI_4$ films. Small and still negative value of β for $EAPbI_3$ excited at 550 nm may be due to the fast saturation of absorption in tail states and may not be directly related with exciton confinement since RSA is owing to either excited state absorption or two-photon absorption. Figure 4(c) shows that the nonlinear refraction effect is also enhanced at low intensity for $EAPbI_3$.

Optics EXPRESS

In order to understand the exciton dynamics in low-dimensional perovskites, the differential absorption spectra of $(BA)_2PbI_4$ and $EAPbI_3$ films are measured by using ultrafast pump-probe measurement. Figure 4(d) illustrates the normalized transient absorption (TA) of perovskite films photoexcited at 400 nm and probed at 500 nm. For low-dimensional perovskites, a sharp negative TA signal due to exciton bleaching quickly recovers within a few picoseconds. In particular, the recovery time of $EAPbI_3$ film is noticeably faster than that of $(BA)_2PbI_4$ film. In Fig. 4(d), the TA signal of three-dimensional $MAPbI_3$ is also exhibited and its relaxation time is much longer (>200 ps) than those of $(BA)_2PbI_4$ and $EAPbI_3$ films. Long lifetime of exciton is beneficial for $MAPbI_3$-based solar cells, but the fast relaxation time is requisite for all-optical switching. Our results open up potential applications for cost-efficient low-dimensional perovskite-based nonlinear optical devices.

4. Conclusion

Through Z-scan measurements and a comprehensive analysis, we have demonstrated that $EAPbI_3$ and $(BA)_2PbI_4$ films with one- and two-dimensional crystal structures have high optical nonlinearities in the visible spectral range. In particular, 1D $EAPbI_3$ has much higher nonlinear optical properties than those of 2D $(BA)_2PbI_4$ and a low saturable intensity near the bandedge. Strong quantum confinement of electrons and holes in the layered $(BA)_2PbI_4$ films leads to a large exciton binding energy and enables intense excitonic emission. Meanwhile, for $EAPbI_3$, 1D chain-like structures constructed via face-shared PbI_6 octahedra are surrounded by organic cations, resulting in a relatively small exciton binding energy, but a large dielectric contrast between them. The large optical nonlinearity of polycrystalline $EAPbI_3$ can thus be attributed to the strong dielectric confinement of excitons along with the quantum confinement. Large nonlinear absorption in 1D $EAPbI_3$ films is less sensitive to the crystalline quality and polycrystalline $EAPbI_3$ films fabricated by the simple spin-coating method show high optical nonlinearities comparable to their single-crystalline counterparts. Our results provide a valuable information for the nonlinear optical application of low-dimensional perovskites in the field of compact and cost-efficient photonic systems.

Funding

Ministry of Science and Technology, Taiwan (107-2112-M-009-015-MY3, 107-2923-M-009-003-MY3); Academia Sinica (AS-CDA-108-M08); Science, Technology and Innovation Commission of Shenzhen Municipality (JCYJ20170818141216288).

Disclosures

The authors declare no conflicts of interest.

References

1. L. Pedesseau, J.-M. Jancu, A. Rolland, E. Deleporte, C. Katan, and J. Even, "Electronic properties of 2D and 3D hybrid organic/inorganic perovskites for optoelectronic and photovoltaic applications," Opt. Quantum Electron. **46**(10), 1225–1232 (2014).
2. L. Dou, A. B. Wong, Y. Yu, M. Lai, N. Kornienko, S. W. Eaton, A. Fu, C. G. Bischak, J. Ma, T. Ding, N. S. Ginsberg, L.-W. Wang, A. P. Alivisatos, and P. Yang, "Atomically thin two-dimensional organic-inorganic hybrid perovskites," Science **349**(6255), 1518–1521 (2015).
3. M. Yuan, L. N. Quan, R. Comin, G. Walters, R. Sabatini, O. Voznyy, S. Hoogland, Y. Zhao, E. M. Beauregard, P. Kanjanaboos, Z. Lu, D. H. Kim, and E. H. Sargent, "Perovskite energy funnels for efficient light-emitting diodes," Nat. Nanotechnol. **11**(10), 872–877 (2016).
4. J. Liu, Y. Xue, Z. Wang, Z.-Q. Xu, C. Zheng, B. Weber, J. Song, Y. Wang, Y. Lu, Y. Zhang, and Q. Bao, "Two-dimensional $CH_3NH_3PbI_3$ perovskite: Synthesis and optoelectronic application," ACS Nano **10**(3), 3536–3542 (2016).
5. B. Li, C. Fei, K. Zheng, X. Qu, T. Pullerits, G. Cao, and J. Tian, "Constructing water-resistant $CH_3NH_3PbI_3$ perovskite films *via* coordination interaction," J. Mater. Chem. A **4**(43), 17018–17024 (2016).

Optics EXPRESS

6. P. Li, Y. Chen, T. Yang, Z. Wang, H. Lin, Y. Xu, L. Li, H. Mu, B. N. Shivananju, Y. Zhang, Q. Zhang, A. Pan, S. Li, D. Tang, B. Jia, H. Zhang, and Q. Bao, "Two-dimensional $CH_3NH_3PbI_3$ perovskite nanosheets for ultrafast pulsed fiber lasers," ACS Appl. Mater. Interfaces **9**(14), 12759–12765 (2017).
7. F. O. Saouma, C. C. Stoumpos, J. Wong, M. G. Kanatzidis, and J. I. Jang, "Selective enhancement of optical nonlinearity in two-dimensional organic-inorganic lead iodide perovskites," Nat. Commun. **8**(1), 742 (2017).
8. W. Liu, J. Xing, J. Zhao, X. Wen, K. Wang, P. Lu, and Q. Xiong, "Giant two-photon absorption and its saturation in 2D organic-inorganic perovskite," Adv. Opt. Mater. **5**(7), 1601045 (2017).
9. I. Abdelwahab, P. Dichtl, G. Grinblat, K. Leng, X. Chi, I. Park, M. P. Nielsen, R. F. Oulton, K. P. Loh, and S. A. Maier, "Giant and tunable optical nonlinearity in single-crystalline 2D perovskites due to excitonic and plasma effects," Adv. Mater. **31**(29), 1902685 (2019).
10. L. N. Quan, M. Yuan, R. Comin, O. Voznyy, E. M. Beauregard, S. Hoogland, A. Buin, A. R. Kirmani, K. Zhao, A. Amassian, D. H. Kim, and E. H. Sargent, "Ligand-stabilized reduced-dimensionality perovskites," J. Am. Chem. Soc. **138**(8), 2649–2655 (2016).
11. C.-W. Lin, F. Liu, T.-Y. Chen, K.-H. Lee, C.-K. Chang, Y. He, T. L. Leung, A. M. C. Ng, C.-H. Hsu, J. Popović, A. Djurišić, and H. Ahn, "Structure-dependent photoluminescence in low-dimensional ethyl-, propyl-, and butylammonium lead iodide perovskites," ACS Appl. Mater. Interfaces **12**(4), 5008–5016 (2020).
12. H. Ahn, M.-T. Lee, and Y.-M. Chang, "Spectral dependence of third-order nonlinear optical properties in InN," Appl. Phys. Lett. **104**(20), 201904 (2014).
13. H. Im, J. Chung, S.-J. Kim, and N.-G. Park, "Synthesis, structure, and photovoltaic property of a nanocrystalline 2H perovskite-type novel sensitizer $(CH_3CH_2NH_3)PbI_3$," Nanoscale Res. Lett. **7**(1), 353 (2012).
14. M. Sheik-Bahae, A. A. Said, T. H. Wei, D. J. Hagan, and E. W. Van Stryland, "Sensitive measurement of optical nonlinearities using a single beam," IEEE J. Quantum Electron. **26**(4), 760–769 (1990).
15. D. Espinosa, L. B. Carlsson, and A. M. Figueiredo Neto, "Influence of nanoparticle size on the nonlinear optical properties of magnetite ferrofluids," Phys. Rev. E: Stat., Nonlinear, Soft Matter Phys. **88**(3), 032302 (2013).
16. B. Gu, Y.-X. Fan, J. Chen, H.-T. Wang, J. He, and W. Ji, "Z-scan theory of two-photon absorption saturation and experimental evidence," J. Appl. Phys. **102**(8), 083101 (2007).
17. K. Wang, H. Long, M. Fu, G. Yang, and P. Lu, "Intensity-dependent reversal of nonlinearity sign in a gold nanoparticle array," Opt. Lett. **35**(10), 1560–1562 (2010).
18. P. Ferrari, S. Upadhyay, M. V. Shestakov, J. Vanbuel, B. De Roo, Y. Kuang, M. Di Vece, V. V. Moshchalkov, J.-P. Locquet, P. Lievens, and E. Janssens, "Wavelength-dependent nonlinear optical properties of Ag nanoparticles dispersed in a glass host," J. Phys. Chem. C **121**(49), 27580–27589 (2017).
19. S. Mirershadi, S. Ahmadi-Kandjani, A. Zawadzka, H. Rouhbakhsh, and B. Sahraoui, "Third order nonlinear optical properties of organometal halide perovskite by means of the Z-scan technique," Chem. Phys. Lett. **647**, 7–13 (2016).
20. M. Sheik-bahae, A. A. Said, and E. W. V. Stryland, "High-sensitivity, single-beam n_2 measurements," Opt. Lett. **14**(17), 955–957 (1989).
21. J. Yi, L. Miao, J. Li, W. Hu, C. Zhao, and S. Wen, "Third-order nonlinear optical response of $CH_3NH_3PbI_3$ perovskite in the mid-infrared regime," Opt. Mater. Express **7**(11), 3894–3901 (2017).
22. S. Kumar, M. Anija, N. Kamaraju, K. Vasu, K. Subrahmanyam, A. Sood, and C. Rao, "Femtosecond carrier dynamics and saturable absorption in graphene suspensions," Appl. Phys. Lett. **95**(19), 191911 (2009).
23. Q. Bao, H. Zhang, Y. Wang, Z. Ni, Y. Yan, Z. X. Shen, K. P. Loh, and D. Y. Tang, "Atomic-layer graphene as a saturable absorber for ultrafast pulsed lasers," Adv. Funct. Mater. **19**(19), 3077–3083 (2009).
24. C.-J. Zhang, K.-X. Guo, and Z.-E. Lu, "Exciton effects on the optical absorptions in one-dimensional quantum dots," Phys. E **36**(1), 92–97 (2007).
25. C. Katan, N. Mercier, and J. Even, "Quantum and dielectric confinement effects in lower-dimensional hybrid perovskite semiconductors," Chem. Rev. **119**(5), 3140–3192 (2019).